American Mineralogist, Volume 91, pages 159–170, 2006

Interstratified kaolinite-smectite: Nature of the layers and mechanism of smectite kaolinization

TERESA DUDEK,[1,*] JAVIER CUADROS,[1] AND SAVERIO FIORE[2]

[1]Department of Mineralogy, Natural History Museum, London, U.K.
[2]Istituto di Metodologie per l'Analisi Ambientale, CNR, Tito Scalo (PZ), Italy

ABSTRACT

This study aims to contribute to a better understanding of the nature and evolution mechanism of interstratified clay minerals. We examined the <2 μm or <0.2 μm size fraction of interstratified kaolinite-smectite (K-S) formed by hydrothermal and hydrogenic alteration of volcanogenic material from a Tortonian clay deposit (Almería, Spain), a weathered Eocene volcanic ash (Yucatan, Mexico), and a weathered Jurassic bentonite (Northamptonshire, England). The methods used were X-ray diffraction analysis (XRD) of random and oriented preparations, thermogravimetry, chemical analysis, and ^{29}Si MAS nuclear magnetic resonance. The proportions of kaolinite and smectite in K-S (%K) were determined by fitting the XRD patterns of ethylene-glycol-saturated samples with patterns calculated with the NEWMOD computer program. The obtained range of compositions is 0–85%K. A comparison of the results from the various techniques showed non-linear relationships, indicating that the layers in K-S are complex and hybrid in nature. The smectite-to-kaolinite reaction is a solid-state transformation proceeding through formation of kaolinite-like patches within the smectite layers. The process consists of several non-simultaneous stages: (1) removal of parts of the tetrahedral sheet, resulting in formation of kaolinite-like patches; (2) layer collapse to ~7 Å where the kaolinite-like patches are sufficiently large; (3) Al for Mg substitution in the octahedral sheet, simultaneous or slightly delayed with respect to layer collapse, causing a layer-charge decrease and loss of interlayer cations; (4) Si for Al replacement in the tetrahedral sheet and further loss of interlayer cations. Iron remains in the kaolinite or is lost at the latest stages of the process.

Keywords: Crystal structure, kaolinite-smectite, solid-state transformation, TGA, XRD

INTRODUCTION

Phyllosilicates are ubiquitous in the Earth's crust. They may be transformed into other phyllosilicates through a sequence of intermediate interstratified phases. Mixed-layer phyllosilicates are critical in many processes (e.g., soil formation, diagenesis, plant growth) and, therefore, they are relevant and fundamental to science and economics. Despite the considerable body of literature on these mineral phases, there is still debate on the nature of the individual layers and what their transformation mechanisms are.

In contrast to phyllosilicate end-members, mixed-layer phases are composed of two or more different layer types that coexist within crystals. The classic interpretation of the nature of mixed-layering assumed that the layers of the interstratification were identical to the end-member species (Weaver 1989). However, several studies of illite-smectite have provided evidence for the existence of "polar layers" (Lagaly 1979; Altaner et al. 1988; Cuadros and Linares 1995; Jakobsen et al. 1995; Stixrude and Peacor 2002), i.e., layers in which the two tetrahedral sheets have different chemical compositions, one smectite-like and the other illite-like, resulting in the two tetrahedral sheets across every interlayer having the same character, smectite-like or illite-like. The implications of this finding are significant because it suggests that the centers of the building process in mixed-layer phyllosilicates are the interlayers, not the layers.

Two mechanisms are usually proposed for phyllosilicate transformation through mixed-layer phases: (1) conversion in the solid-state by atom rearrangement with the interlayer as the main route for atom diffusion in and out the structure; (2) dissolution of the original mineral and crystallization of the new structure. Evidence for both mechanisms has been reported (solid-state transformation of illite-smectite: Cuadros and Altaner 1998; Lindgreen et al. 1991, kaolinite-smectite: Amouric and Olives 1998; Hughes et al. 1993, biotite-vermiculite: Środoń 1999, and dissolution-crystallization of illite-smectite: Inoue et al. 1988; Środoń et al. 2000, kaolinite-smectite: Środoń 1980; Delvaux et al. 1989, glauconite-smectite: Buatier et al. 1993). It seems that the solid-state transformation mechanism prevails in weathering environments. In diagenetic and hydrothermal environments, the occurrence of either solid-state transformation or dissolution-crystallization appears to be largely controlled by fluid/rock ratio, with a high ratio favoring dissolution-crystallization. In our view, the solid-state transformation mechanism is more consistent with a polar layer structure and the central role of the interlayer in the reaction, because it suggests that the reaction occurs in the limited tetrahedral-interlayer-tetrahedral region, rather than affecting entire crystals, as dissolution would do.

The purpose of the present study was to investigate the possible layer polarity of kaolinite-smectite (K-S) and the mechanism of K-S formation and evolution. We chose to examine K-S because the very different structure (1:1 vs. 2:1) and composition

* E-mail: T.Dudek@nhm.ac.uk

0003-004X/06/0001–159$05.00/DOI: 10.2138/am.2006.1897

of the kaolinite and smectite layers allows a crystal-chemical study with minimum ambiguity. Also, a possible polar character of such different layers would make a strong case for "layer polarity" as an intrinsic feature of mixed-layer phyllosilicates.

K-S has been reported commonly in soils as an intermediate product of the conversion of smectite into kaolinite (e.g., Buhmann and Grubb 1991; Churchman et al. 1994; Hughes et al. 1993). The investigation of K-S is then also relevant for soil preservation, because smectite kaolinization impoverishes soils by substituting smectite, which is able to retain and release water and nutrients, with kaolinite, an inert soil component. The solid-state transformation mechanism of this reaction, by stripping of one of the tetrahedral sheets, has been supported by high-resolution transmission electron microscopy (HRTEM) images (Amouric and Olives 1998) and chemical data showing that Ti and Fe were preserved in the newly formed kaolinite layers (Hughes et al. 1993). Iron-rich K-S also was reported by Carson and Kunze (1967). In contrast, Delvaux et al. (1989), using electron spin resonance spectroscopy, found a low Fe content in K-S originating from Fe-rich smectite. They suggested that the K-S formation process involves the destruction of 2:1 smectite layers and subsequent neoformation of kaolinite and Fe oxides. The dissolution-crystallization mechanism was also suggested by Środoń (1980) on the basis of hydrothermal experiments. However, Wiewióra (1973) and Sakharov and Drits (1973) postulated direct crystallization of K-S from solution, without a smectite precursor, during hydrothermal alteration of volcanic material.

The results of our study show that mixed-layering in K-S is more complex, from both the chemical and structural viewpoint, than previous descriptions of mixed-layer phyllosilicates. The individual layers appear partially stripped of one of the tetrahedral sheets and the chemical and structural changes do not progress simultaneously. A solid-state transformation is the most likely mechanism leading to the development of such a complex structure.

Materials and methods

Twenty-two K-S samples from three different localities were studied. Twenty specimens are from the Los Trancos bentonite deposit in Almería, SE Spain, which developed by hydrothermal alteration of amphibolitic dacite agglomerates and tuffs (Linares 1985). The volcanic activity that produced these rocks occurred during the Middle-Upper Tortonian. The hydrothermal solutions, which reached temperatures of about 70 °C, were of meteoritic origin (Linares 1985). The characteristic feature of these deposits is an abundant occurrence of low-temperature tridymite, which precipitated syngenetically with the bentonite (Linares 1985). Three of the Almería samples are palaeosols developed on bentonites; the rest were formed by hydrothermal activity. Two other palaeosol samples were analyzed: one from the Yucatan Peninsula, Mexico, formed by weathering of Eocene volcanic ash (Schultz et al. 1971), and the other one from Rushden, Northamptonshire, U.K., developed on a Jurassic bentonitic bed (Hillier et al. 2002).

The <2 μm particle size fraction (<0.2 μm for sample RS49) was separated from the bulk samples by dispersion in water and sedimentation according to Stoke's law. Aliquots of the separated fraction were Li- and Ca-saturated in the exchangeable cation sites by dispersion in 3 *M* LiCl and 0.1 *M* $CaCl_2$ solutions, respectively. The specimens from England and Mexico were pre-treated by the ammonium oxalate (Smith 1994) and the dithionite-citrate-bicarbonate (Jackson 1975) methods, respectively to remove amorphous Fe phases. Samples from the area where the Mexico specimen was collected showed <1 wt% of amorphous $SiO_2 + Al_2O_3$ (Schultz et al. 1971).

X-ray diffraction (XRD) analysis was performed at the Natural History Museum, London, U.K., using a Philips PW1050 diffractometer operating under the following conditions: 42 kV, 42 mA, Cu radiation, graphite secondary monochromator, 1° divergence slit, and 0.1 mm receiving slit. The Li-saturated samples were analyzed in two types of experiments: (1) oriented aggregates prepared by sedimentation on glass slides (10 mg sample/4 cm^2) and analyzed in air-dried and glycolated forms (overnight saturation in ethylene glycol atmosphere at 60 °C) from 3 to 30 °2Θ, at 0.05 °2Θ/step and 10 s counting time; and (2) randomly oriented aggregates prepared by side-loading and scanned from 19 to 85 °2Θ, at 0.06 °2Θ/step and 60 s counting time. The proportion of kaolinite and smectite layers in K-S (percent kaolinite layers, %K) was calculated by fitting the experimental ethylene-glycol- saturated patterns with those calculated with the NEWMOD computer program (Reynolds and Reynolds 1996). This method is based on the variations in the position and shape of the 00*l* K-S peaks, which are controlled by the proportion of layers with different basal spacings (~7 Å for kaolinite and ~17 Å for ethylene-glycol-solvated smectite). Modeling of air-dried XRD patterns of K-S samples with NEWMOD proved unsuccessful (see results).

Thermogravimetric analysis (TG) was performed at the Istituto di Metodologie per l'Analisi Ambientale, CNR, Potenza, Italy, using a Seiko Exstar 6000 apparatus. The samples were heated in Al_2O_3 crucibles from 20 to 1050 °C at 10 °C/min in a N_2 flow. Sample weights ranged from 9 to 15 mg. The dehydroxylation weight loss was measured from the TG curves, after discrimination from hydration water loss. The derivatives of the TG diagrams were calculated (DTG), and the part of the curves corresponding to the dehydroxylation events was decomposed into several dehydroxylation peaks by curve-fitting using the computer program Galactic Grams/AI (version 7.01). The decomposition was performed using Gaussian-shaped peaks.

^{29}Si magic-angle spinning nuclear magnetic resonance (^{29}Si MAS-NMR) spectra were recorded at the Department of Earth Sciences of the University of Cambridge on a Varian-CMX Infinity spectrometer with a magnetic field of 9.4 T, at a radiofrequency of 79.47 MHz, in 7.5 mm rotors. A rotation speed of 6 kHz was employed. Spectra were obtained using π/9 single-pulse excitation with pulse duration of 1 μs and 60 s delay time. The latter parameter was selected after ensuring full signal recovery by performing experiments of ≤180 s delay time. Spectra were referenced to tetramethylsilane (TMS). The experimental spectra were decomposed by curve-fitting with the software indicated above. In this case, the peaks were first deconvoluted to identify the position of the maxima, because they were not sufficiently resolved. For sample LT-10/6, the deconvolution was not possible owing to low signal-to-noise ratio, and the positions of the bands were assumed to be the same as for the other samples. We used Gaussian-Lorentzian functions with a 20% contribution from the latter.

Chemical analyses, including cation exchange capacity (CEC), of the Los Trancos specimens are from Reyes et al. (1978) and Cuadros et al. (1994). Amorphous phases typically are <1 wt% SiO_2, <0.4 wt% Fe_2O_3, and <0.5 wt% Al_2O_3. The Mexico and England specimens were analyzed in the Natural History Museum using an ICP-AES Varian Vista Pro apparatus after dilution in $LiBO_2$ (1:5), fusion, and dissolution in HNO_3.

Results

XRD patterns of the oriented mounts

The NEWMOD-calculated compositions of K-S samples and the parameters used for the calculations are shown in Table 1. Figure 1 shows selected examples of the XRD experimental and modeled patterns. A satisfactory fit for peak positions and widths was obtained for all samples. However, we encountered problems with the fitting of the background, especially in the low-angle region. For the most kaolinitic samples, RS49 and CWP-73, there is also a misfit in the intensity of the peak around 26 °2Θ, which we were not able to simulate.

For eight samples, there was a good fit of the experimental and theoretical patterns using one phase (smectite or K-S; Figs. 1a and 1e). For the other twelve samples, two or three phases were required, including K-S of different composition (kaolinite-poor: <50%K, and kaolinite-rich: >50%K), smectite, and, in two cases, kaolinite and illite (Figs. 1b, 1c, and 1d). K-S with <50% K was a dominant component of the mixtures, comprising 55–90 wt% (Table 1). This heterogeneity may be related to the differential transformation of smectite to kaolinite within a confined space.

TABLE 1. The NEWMOD-calculated compositions of the K-S samples and the parameters used for the modeling

Sample	Total %K	Phase	%K in each phase	wt% of phase	d_K (Å)	N_{avg}	N
TR-4	0	smectite	–	100	–	2.5	1-10
TR-146	0	smectite	–	100	–	2.5	1-10
T-21	7	K-S	7	100	7.4	2.5	1-10
TR-3	7	K-S	7	100	7.4	2.5	1-10
T-16	10	K-S	10	100	7.4	2.5	1-10
TR-2	13	K-S	13	100	7.4	2.5	1-10
LT-9/1	16	K-S	10	90	7.4	2.5	1-10
		K-S	60	10	7.15	2.5	1-10
T-22	25	K-S	13	70	7.4	2.5	1-10
		K-S	50	30	7.4	2.5	1-10
LT-10/6	32	K-S	20	60	7.4	2.5	1-10
		K-S	60	30	7.15	2.5	1-10
		smectite	–	10	–	2.5	1-10
TR-119	32	K-S	20	80	7.4	2.5	1-10
		K-S	70	20	7.15	2.5	1-14
TR-125	32	K-S	15	65	7.4	2.5	1-10
		K-S	60	35	7.15	2.5	1-10
LT-9/3	33	K-S	25	75	7.4	2.5	1-10
		K-S	60	20	7.15	2.5	1-10
TR-115	34	K-S	25	60	7.4	2.5	1-10
		K-S	60	30	7.15	2.5	1-10
		smectite	–	10	–	2.5	1-10
T-18	37	K-S	20	70	7.4	2.5	1-10
		K-S	70	30	7.15	2.5	1-14
TR-117	38	K-S	38	100	7.4	2.5	1-10
LT-9/2	39	K-S	25	55	7.4	2.5	1-10
		K-S	60	35	7.15	2.5	1-10
		smectite	–	10	–	2.5	1-10
T-20	47	K-S	30	70	7.4	2.5	1-10
		K-S	80	30	7.15	2.5	1-14
TR-121	49	K-S	40	85	7.4	2.5	1-10
		K-S	90	15	7.15	2.5	1-14
LT-2	55	K-S	40	75	7.4	2.5	1-10
		K-S	90	25	7.15	2.5	1-14
LT-10/1	61	K-S	30	55	7.4	2.5	1-10
		K-S	90	42	7.15	2.5	1-14
		kaolinite	100	3	7.12	10	1-55
RS49	80	K-S	80	100	7.15	3	1-14
CWP-73	85	K-S	85	90	7.15	2.5	1-14
		Illite	–	10	–	4	1-14

Notes: d_K = *d*-value of kaolinite layers; N_{avg} and N = mean number of layers and range of number of layers in the coherent scattering domains. Other parameters used for modeling: *d*-value of ethylene-glycol solvated smectite layers = 16.7 Å (for RS49 and CWP-73 = 16.9 Å); *d*-value of illite (sample CWP-73) = 9.94 Å; ordering: R0, for CWP-73 and RS49 = R1; σ* = 30.

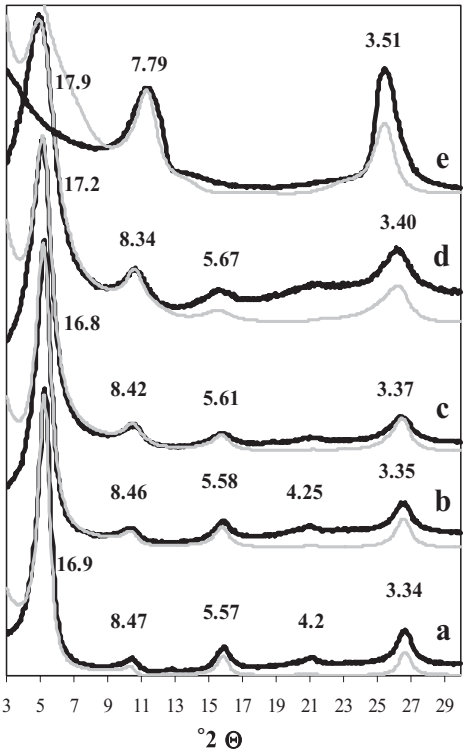

FIGURE 1. Selected XRD patterns of the oriented, ethylene-glycol-solvated K-S samples and their NEWMOD-modeled traces (black: experimental, gray: calculated). Peak positions in angstroms; (**a**) smectite, TR-4; (**b**) 16%K, LT-9/1; (**c**) 32%K, TR-125; (**d**) 49%K, TR-121; (**e**) 80%K, RS49.

However, the model of phase mixing used to simulate this heterogeneity probably does not represent the exact composition of the corresponding samples.

Some of the parameters used in the NEWMOD calculations are different for kaolinite-poor and kaolinite-rich K-S. The kaolinite basal spacings were 7.4 and 7.15 Å for the K-S phases with <50%K and >50%K, respectively. Also, the number of layers in the coherent scattering domain (N) ranged from 1 to 10 and from 1 to 14 for the kaolinite-poor and kaolinite-rich K-S phases, respectively. The 7.15 Å *d*-spacing and larger coherent scattering domain in kaolinite-rich phases indicate more perfect kaolinite layers. The *d*-value of ethylene-glycol-saturated smectite was 16.9 Å for samples RS49 and CWP-73, and 16.7 Å for the other samples. The layer stacking was ordered (R1) for samples RS49 and CWP-73, and random (R0) for the other specimens. The same particle-orientation parameter, σ* = 30, was applied to all samples (σ* is the standard deviation of the orientation of crystals from the substrate plane; Moore and Reynolds 1997). We introduced into the calculations the values for the goniometer radius (17.3 cm) and sample length (2.5 cm) from our diffractometer. The Fe content of smectite was obtained from the chemical data, recalculated for the half formula unit of a 2:1 dioctahedral clay structure. The Fe content of our samples ranges from 0.03 to $0.2/O_{10}(OH)_2$. We assigned all Fe identified in a given sample to smectite layers, although this may not be the case, especially for samples containing more kaolinite. We found, however, that the patterns calculated using different Fe contents (from within the range of Fe values in our samples) were essentially identical. Kaolinite layers were calculated without Fe. We also tested the effect of Fe in kaolinite on the XRD patterns, because, as shown below, some Fe is retained in the kaolinite layers during the smectite-to-kaolinite transformation. As NEWMOD does not allow manipulating the chemical composition of kaolinite, the test was performed using serpentine layers with the Fe content taken from the chemical analysis, assuming the same Fe content in smectite and kaolinite. Negligible differences between the patterns calculated using Fe-free kaolinite and serpentine were observed.

The 7.4 Å *d*-value of the kaolinitic layers in K-S with <50%K may suggest that these layers are non-expanding halloysite rather than kaolinite (e.g., Brown and Brindley 1980). There are three methods to differentiate halloysite from kaolinite: (1) the formamide, (2) K-acetate, and (3) hydrazine hydrate (reviewed in Theng et al. 1984). Each causes expansion of smectite layers, and therefore they are not suitable for K-S samples. In contrast, Brindley (1980) suggested that halloysite is a highly disordered form of kaolinite and, in K-S of low kaolinite content, disordered

kaolinite layers are more likely to be present than well-crystallized kaolinite layers. As it is not possible to discriminate between the two, for simplicity, we refer to the 7.4 Å component as kaolinite, consistent with previous studies describing K-S. Also, in view of our interpretation (see discussion), the differences between kaolinite and halloysite in a K-S structure are vague.

As mentioned above, we could not obtain satisfactory results for the modeling of air-dried XRD patterns. This is probably related to a non-uniform hydration state of smectite layers in K-S, leading to mixed-layer sequences with more than two components (kaolinite and smectite in several hydration states). The version of NEWMOD used can model only two-component sequences.

XRD patterns of randomly oriented aggregates

Figure 2 shows diffraction patterns of randomly oriented aggregates in the sequence from smectite (Fig. 2a) to 80%K (Fig. 2e), where %K refers to the NEWMOD-calculated value. Asymmetric two-dimensional 02;11 and 20;13 reflections and the 06 peak are the main non-basal peaks identified in all patterns. Only very broad tri-dimensional reflections appear in the most kaolinitic sample (Fig. 2e). These features indicate very limited development of tri-dimensional ordering during the transformation from smectite to kaolinite.

The region of the patterns containing the 06 peaks is presented in Figure 3. The K-S samples show only one maximum, in contrast, a physical mixture containing 25 wt% of smectite and 75 wt% of kaolinite, has two distinct maxima (Fig. 3f).

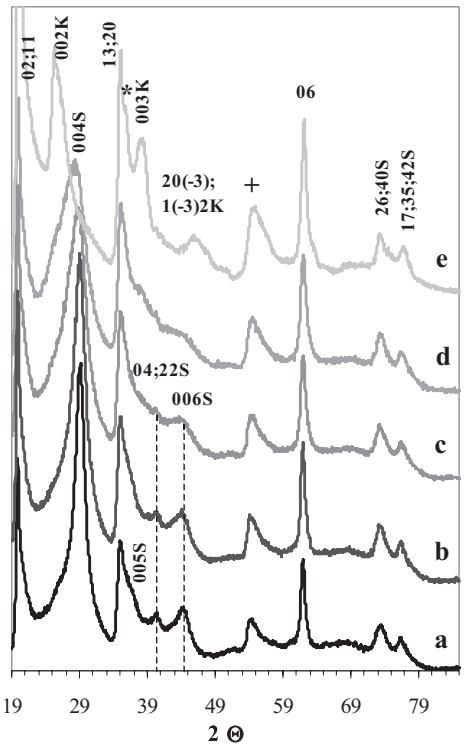

FIGURE 2. Selected XRD patterns of randomly oriented K-S samples (one-water layer smectite). Two-dimensional diffraction bands are labeled with *hk* indices. S = smectite; K = kaolinite; * 1($\bar{3}$)($\bar{1}$);20 K; + 15;24;31 S / 24($\bar{1}$);20($\bar{4}$);1($\bar{3}$)3;151 K. The samples are those in Figure 1.

Such behavior indicates that our samples consist of an intimate combination of kaolinite and smectite layers or domains within the crystals, rather than a mixture of crystals of the two phases. The position of the 06 peaks migrates from values characteristic of smectite (Fig. 3a) to those of kaolinite (Fig. 3e). The width of the peaks increases with increasing %K, to 60%K (Figs. 3a–3d), and then decreases (Fig. 3e). Thus, the width of the 06 peaks changes according to the changing contribution of kaolinite and smectite: it is smallest where either of the two components is dominant and the largest where they are present in approximately equal amounts.

Dehydroxylation of the octahedral sheet

The TG curves of our samples (Fig. 4) show dehydration and dehydroxylation events. The inflection point after the constant weight decrease was chosen as the onset of dehydroxylation. The weight loss before the inflection point corresponds to dehydration. For our samples, the temperature of the transition between dehydration and dehydroxylation ranges from ~260 to 400 °C. We calculated the weight loss of the samples owing to dehydroxylation of the octahedral sheet as shown in Figure 4. As %K increases, the dehydroxylation weight loss increases and the onset of dehydroxylation moves to lower temperature. Our samples show three dehydroxylation events: at ~450 °C for kaolinite, ~620 °C for smectite, and ~550 °C for an "intermediate" component (Fig. 5). These values are lower than some others reported in the literature because N_2 flow reduces dehydroxylation temperatures. Dehydroxylation DTG peaks are asymmetric because the reaction is accelerated as temperature rises. Therefore, to decompose these peaks, we used more than one Gaussian curve for each real dehydroxylation component whenever the curve-fitting process required it. As the components overlap, it is impossible to be certain of the shape of each, and the determination may not be accurate. The contributions

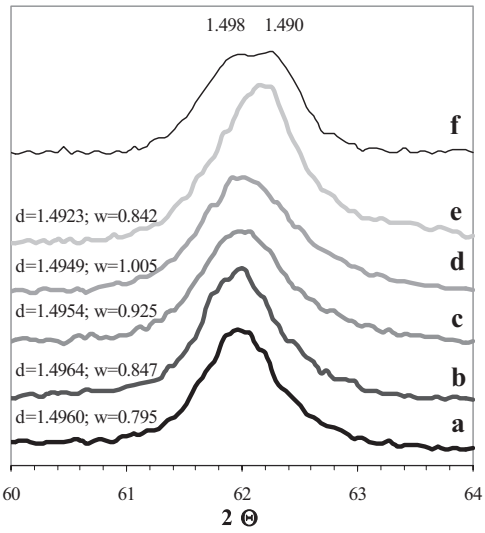

FIGURE 3. 06 reflection from the XRD patterns of randomly oriented aggregates; (**a**–**e**) K-S samples as in Figure 1; (**f**) physical mixture with 75 wt% of smectite and 25 wt% of kaolinite. *d* (*d*-values) and *w* (width) of the peaks in Å and Δ°2Θ, respectively; 1.498 and 1.490 Å are the *d*-values of smectite and kaolinite in the mixture, respectively.

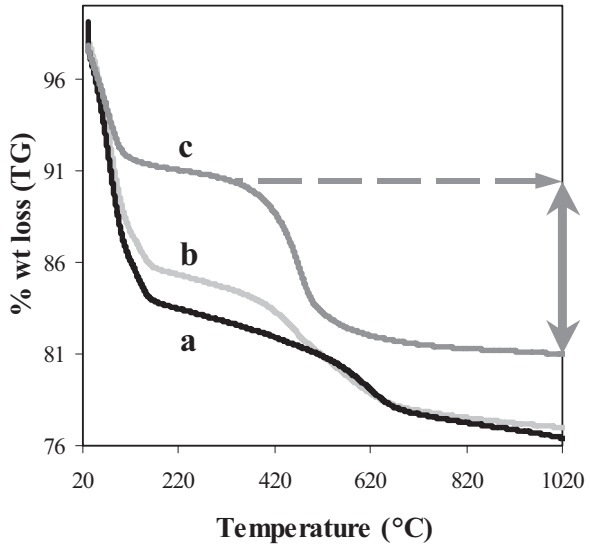

FIGURE 4. Selected TG curves of the studied samples. (**a**) smectite, TR-4; (**b**) 47%K, T-20; (**c**) 80%K, RS49. Trace c shows how the percent weight loss corresponding to dehydroxylation was measured.

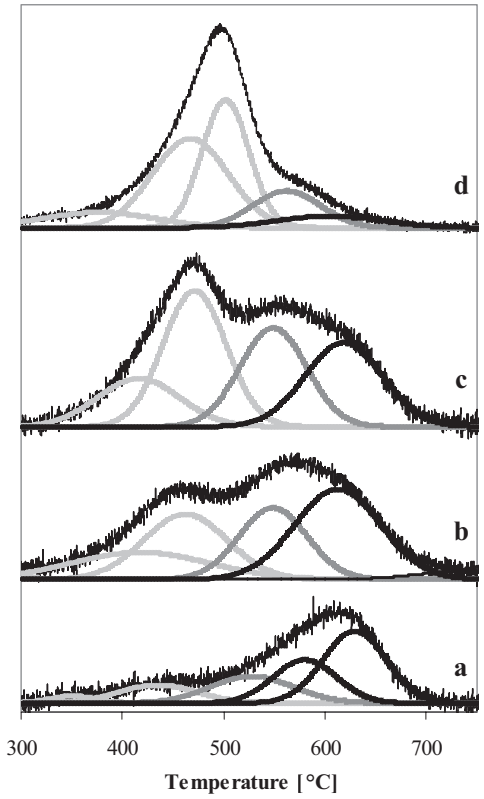

FIGURE 5. Parts of the DTG curves corresponding to the dehydroxylation of the octahedral sheet and their decomposition. Three dehydroxylation events with maxima at about 450, 620, and 550 °C corresponding to smectite (black line), kaolinite (light gray line) and "intermediate" (dark gray line) were recognized. Each event is simulated with one or more curves (see text). (**a**) smectite, TR-4; (**b**) 32%K, TR-125; (**c**) 47%K, T-20; (**d**) 85%K, CWP-73.

of these components to the total dehydroxylation event evolve regularly during the transformation of smectite to kaolinite. With increasing %K, there is a decrease in the area of the smectite peaks and an increase of the kaolinite peaks. We detected a kaolinite component in the DTG diagrams of samples TR-4 and TR-146, whereas XRD detected only smectite layers. Also, the contribution from the "intermediate" component increases initially (Figs. 5a–5c), to about 60%K, and then decreases (Fig. 5d). The dehydroxylation weight loss of the "intermediate" component was calculated using the area under the peak, which was then normalized by division by the sample dry weight. The nature of the intermediate component will be addressed in the discussion section.

^{29}Si MAS NMR

The ^{29}Si MAS NMR analyses (Fig. 6) were performed for four samples: TR-4 (smectite), LT-10/6 (32%K), LT-2 (55%K), and RS49 (80 %K). Each spectrum was fitted with three peaks whose maxima were identified by deconvolution at about –87, –91, and –94 ppm. The two latter peaks correspond to Q^3(0Al) Si sites in kaolinite (Sherriff et al. 1991) and smectite (Trillo et al. 1993), respectively. Therefore, there is an indication that there are kaolinite domains in samples where XRD only detects smectite layers. The Q^3(0Al) sites represent tetrahedral Si with three other Si atoms as nearest-neighbors in tetrahedral positions. The peak at –87 ppm corresponds to two sites: Q^3(1Al), i.e.,

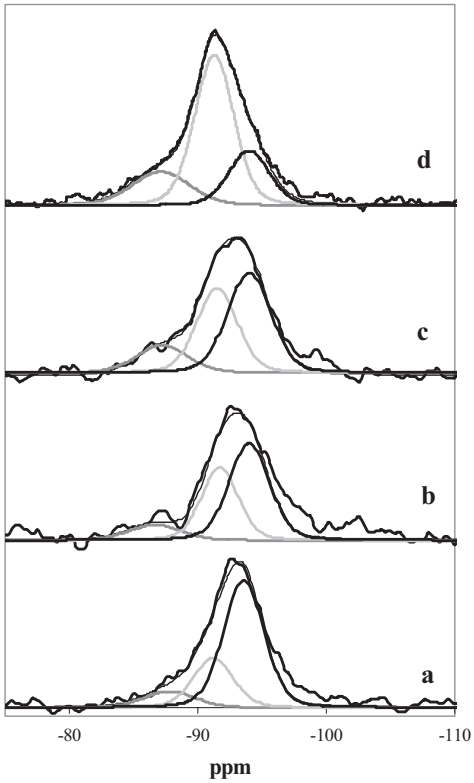

FIGURE 6. ^{29}Si MAS NMR spectra of the four studied samples. (**a**) smectite, TR-4; (**b**) 32%K, LT-1/6; (**c**) 55%K, LT-2; (**d**) 80%K, RS49. The three components correspond to Q^3(0Al) site in smectite (black line), Q^3(0Al) site in kaolinite (light gray line), and a mixture of Q^3(1Al) and Q^2(0Al) sites (dark gray line).

Si surrounded by two Si atoms and one Al atom in tetrahedral positions and $Q^2(0Al)$, Si with only two Si neighbors (crystal edges and defects within the crystal structure). The positions of the peaks were fixed during curve fitting after obtaining their positions from a deconvolution procedure. In all samples, the width of both Q^3 peaks (at –91 and –94 ppm) was maintained constant. The width of the peak at –87 ppm was assumed to be larger than the width of the Q^3 peaks because there are two components in this peak. We did not try to fit the area between –97 and –100 ppm in Figures 6a–6c because, to our knowledge, no peak exists in this region. Also, the "extra" intensity in this region appears to be an artifact of the low signal-to-noise ratio. The different signal-to-noise ratio in the spectra was caused by the different amounts of sample available for analysis.

The relative intensities of the three peaks vary regularly with the changing proportion of kaolinite:smectite in K-S. With increasing %K, the intensity of the kaolinite peak at –91 ppm increases at the expense of the smectite peak at –94 ppm. The area of the –87 ppm peak slightly increases with increasing %K. Note that sample RS49 contains considerably smaller crystals (<0.2 μm) than the other samples (<2 μm). Therefore, the contribution of crystal edges to the $Q^2(0Al)$ peak is expected to be much greater. The relative intensities were measured only for the central bands, because the spinning side bands had very small signal-to-noise ratio.

Chemistry

Table 2 presents the chemical data for the studied samples (arranged according to increasing %K) as wt% oxides and CEC. The sum of oxides for samples RS49 and CWP-73 is not 100% because H_2O was not measured. There is a trend of decreasing MgO with increasing proportion of kaolinite layers in K-S. Also, SiO_2 and CEC decrease and Al_2O_3 increases with increasing %K, although these trends are not as evident. The remaining metal oxides, including Fe_2O_3, do not show any trend for the studied suite of samples. Note the high Fe_2O_3 content in the kaolinitic samples. Also, there is no increase in H_2O content with increasing %K, as expected. The reason for this is that H_2O measurements were performed after overnight heating of samples at 100 °C, therefore, they still contained hydration H_2O, which needs a higher temperature to be removed completely. The wt% H_2O in Table 2 is then a combination of hydration and hydroxyl water. As the variation of both components with increasing %K is opposite, there is no resulting trend.

Discussion

Kaolinite and smectite layers or domains in the K-S structure

Because the 06 reflection has a single maximum (see Fig. 3), grains consist of an intimate combination of kaolinite and smectite layers or domains, rather than a mixture of two types of crystals. This conclusion is reinforced by the evolution of the width of the 06 peaks with increasing %K calculated from XRD (Fig. 7). As noted above for the selected samples in Figure 3, the width of the 06 peaks for each studied specimens increases to 60%K and then decreases. The wider peak is related to the contribution of the smectite and kaolinite peaks. The effect is similar to that for the basal reflections in mixed-layer minerals: 00*l* peaks change position and broaden when peaks of two or more components are sufficiently close to merge and create one peak. In the case of the 06 reflection, there are kaolinite and smectite layers in the same crystal or domains in the same layer (see below), which generate one single 06 peak, although this peak is wider and with a maximum that moves in position from that of smectite to that of kaolinite as %K increases.

The maximum width of the 06 peak is expected at ~50%K, where both peaks have similar intensity, or even at lower %K values, because kaolinite has a greater diffracting power than smectite. However, the widest measured 06 peaks correspond to %K > 50. This behavior occurs because some samples have K-S of various compositions, some with >50% kaolinite layers, which increases the %K values of these samples. However, the width of the 06 peak is controlled by the phase with the widest peak, provided it is present in sufficient concentration.

Table 2. Chemical analysis (wt% oxide) and CEC (meq/100g) of the K-S samples

	$\%K_{XRD}$	SiO_2	Al_2O_3	Fe_2O_3	TiO_2	CaO	MgO	Na_2O	K_2O	H_2O	sum	CEC
TR-4	0	60.0	21.1	1.2	0.3	1.3	6.3	1.4	0.2	9.8	101.6	110
TR-146	0	61.6	18.2	2.7	0.2	1.4	6.2	0.1	0.3	9.2	99.8	116
T-21	7	57.2	21.7	2.3	n.d.	1.8	5.9	0.8	0.2	11.1	100.8	113
TR-3	7	58.3	22.5	1.3	0.3	1.2	5.8	1.5	0.1	9.4	100.3	118
T-16	10	55.3	22.4	2.4	n.d.	1.6	5.6	1.1	0.1	10.7	99.6	118
TR-2	13	57.7	24.2	1.3	0.3	1.1	5.3	1.6	0.1	9.7	101.3	89
LT-9/1	16	58.1	22.4	1.0	0.0	1.8	5.5	1.7	0.3	8.1	98.9	104
T-22	25	57.5	21.2	2.3	n.d.	0.9	5.6	0.9	0.2	12.0	100.5	93
LT-10/6	32	58.8	22.8	0.7	0.0	1.5	4.9	1.1	0.2	9.0	99.0	84
TR-119	32	59.6	23.4	2.7	0.2	1.2	4.3	0.2	0.1	9.5	101.1	108
TR-125	32	58.8	24.1	2.7	0.2	1.1	4.5	0.1	0.1	9.6	101.3	99
LT-9/3	33	58.7	22.3	1.1	0.0	1.6	5.0	1.8	0.3	8.9	99.7	107
TR-115	34	58.4	23.7	2.7	0.2	1.2	4.4	0.2	0.1	9.4	100.3	108
T-18	37	55.4	23.3	2.9	n.d.	1.2	5.5	0.7	0.2	11.6	100.8	102
TR-117	38	56.6	24.7	3.0	0.2	1.1	3.8	0.1	0.1	10.3	99.7	90
LT-9/2	39	58.1	22.4	1.9	0.0	1.9	4.3	1.6	1.3	9.1	100.5	101
T-20	47	55.0	21.8	3.9	n.d.	1.1	5.0	0.7	0.2	12.4	100.1	82
TR-121	49	57.1	24.1	2.9	0.2	1.1	3.7	0.1	0.1	10.5	99.7	90
LT-2	55	54.9	25.1	2.1	n.d.	1.9	3.8	1.3	0.3	10.3	99.7	94
LT-10/1	61	55.0	24.6	1.6	0.0	2.1	3.8	1.4	0.3	10.6	99.3	81
RS49	80	43.4	26.9	3.7	0.3	0.1	0.8	1.2	1.0	n.d.	77.2	21
CWP-73	85	44.7	28.4	2.1	1.0	0.1	0.6	1.5	1.1	n.d.	79.5	25

Notes: MnO and P_2O_5 were <0.008 and <0.023, respectively; n.d. = not determined. The CEC values for samples RS49 and CWP-73 were calculated from the wt% oxide data.

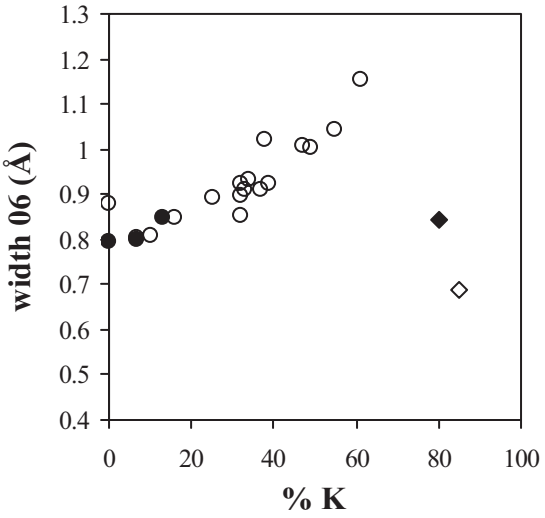

FIGURE 7. Width of the 06 peak from the randomly oriented XRD aggregates as a function of %K layers in K-S (XRD measurements). Full circles: Almería specimens formed in soil developed on bentonites; hollow circles: Almería specimens formed by hydrothermal alteration of volcanogenic material; hollow diamond: England specimen; full diamond: Mexico specimen.

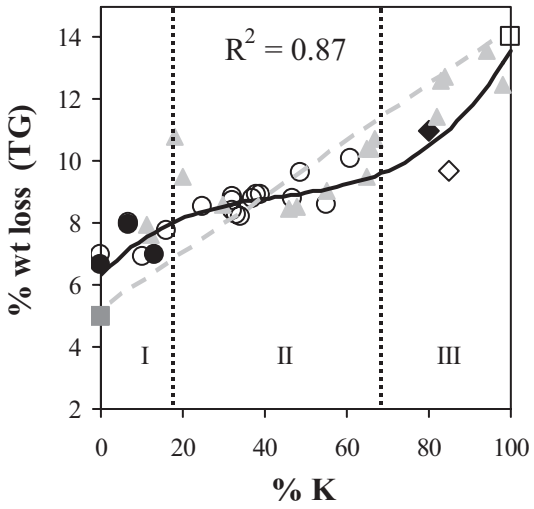

FIGURE 8. Percent weight loss due to dehydroxylation of the octahedral sheet (TG analysis) vs. %K in K-S (XRD measurements). Symbols as in Figure 7. Additional symbols: full square: ideal value for smectite; hollow square: ideal value for kaolinite; gray triangles: samples from Brindley et al. (1983). During smectite kaolinization, the number of OH groups in K-S does not increase proportionally to the relative amount of kaolinite layers as measured by XRD (the dashed line shows the hypothetical linear relation, for comparison). The trend is divided into three stages (see text for explanation).

Transformation from a 2:1 to 1:1 structure

Figure 8 shows the relationship between weight loss resulting from the dehydroxylation of the octahedral sheet (TG data), and %K (XRD data, Table 1) for the samples in this study (circles and diamonds) and K-S samples from palaeosols developed on chalk- and silica-rich rocks in the Paris Basin (Brindley et al. 1983) (triangles). The latter authors used two methods based on the analysis of the XRD patterns of glycol-saturated samples to determine kaolinite:smectite layer proportion, both of which provided very similar results. Figure 8 also shows the theoretical values for smectite (montmorillonite composition) and kaolinite (full and open square, respectively). The regression curve is calculated only for our samples, including the theoretical smectite and kaolinite values. The dashed gray line shows the linear trend between the two represented variables.

In Figure 8, weight loss, which is a measure of the OH increase during the transformation from smectite to kaolinite, is not related linearly to the evolution of K-S composition recorded by XRD. The two sets of samples plotted show similar trends, in which three stages can be recognized: (I) = 0–20%K, a sharp increase in the number of OH groups; (II) = 20–70%K, very little OH increase; (III) = 70–100 %K, sharper increase in the number of OH groups. This behavior indicates that layers that have not collapsed to ~7 Å contain an OH "excess." In other words, the layers are not entirely smectitic or kaolinitic. Thus, it seems that smectite-to-kaolinite conversion does not occur in the simple layer-by-layer replacement but through the development of patches within smectite layers where part of the tetrahedral sheet is stripped off and OH groups are attached (Fig. 9). The patches have the 1:1 structure, although they do not necessarily yield a ~7 Å kaolinite *d*-value (henceforth they are called "kaolinite-like patches"). At the beginning of the transformation process (stage I of Fig. 8), the patches are small and there is little change

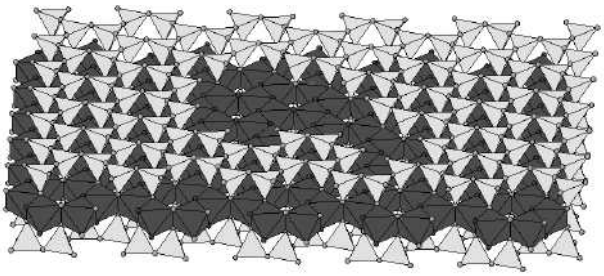

FIGURE 9. Sketch of a smectite 2:1 layer during the transformation to kaolinite. Some tetrahedra have been removed from the central area of the layer, which becomes a kaolinite-like patch. Kaolinization proceeds by the formation and growth of these kaolinite-like patches.

in the basal spacing. As the transformation proceeds, the patches become sufficiently large to allow formation of ~7 Å domains or layers, producing interstratification. In stage II (~20–70%K), layer collapse involves comparatively little exchange of tetrahedra by OH groups. Finally (stage III), the remaining layers or domains collapse to ~7 Å following a significantly larger substitution of tetrahedra by OH groups. Because ~45% of this latter substitution occurs while only ~20% of layers collapse, much of this latter substitution probably occurs on the external crystal surface (rather than interlayers) where it has a reduced effect on basal spacing. Part of the tridymite found in the Almería samples (Linares 1985) is probably the product of this silica loss.

There is an uncertainty in the %K calculation in NEWMOD that is difficult to assess. However, we are confident that this uncertainty does not alter the essential shape of the plot in Figure 8. For example, we modeled the XRD patterns of the K-S

samples with one K-S phase. The maximum differences in %K were 10%. However, the shape of the plot remained similar to that in Figure 8.

To ascertain the validity of this interpretation, we modeled the relationship between OH loss and layer collapse (Fig. 10). We assumed that the external sides of the crystals do not undergo transformation into kaolinite (stripping of the tetrahedral sheet) until all the internal layers have transformed. There is experimental evidence of kaolinite crystals with smectite layers at the edges (Ma and Eggleton 1999). Hence, the transformation is modeled in two stages, corresponding to internal and external layers. The model is sensitive to the number of layers per crystallite and the only good fit to the experimental results in Figure 8 was obtained with crystals containing three layers. Interestingly, our NEWMOD simulations of the XRD patterns indicated that the crystals have a mean number of 2.5 layers. Internal layers contribute their total surface to both hydroxyl loss and layer collapse. External layers contribute also in terms of hydroxyl loss but not to layer collapse because only part of the external surfaces rest flat on another crystal in the oriented mount and generate XRD intensity. We assumed that only 30% of the external surface of each crystal contributes to XRD intensity.

Initially, there is partial stripping of the tetrahedral sheets from the internal layers without layer collapse. Thus, in our model, there is a weight loss to 6% without layer collapse. From this point on, further growth of the kaolinite-like patches in the internal layers causes partial collapse. Initially, the collapse is much less than the total size of the kaolinite-like patches but, as the patches become larger, greater areas of the layers collapse. Thus, we modeled this part of the plot assuming an exponential increase of layer collapse (K) as a function of the increase in the total area of the kaolinite-like patches (A), i.e., $K = A^{1.22}$. This behavior ceases when the patches are sufficiently large that layer collapse occurs in the entire area of the patches. In our model, this occurs at ~10% weight loss, which corresponds to 80% of the interlayer area now being part of kaolinite-like patches. From this point on, the removal of tetrahedral sheets in the internal layers and layer collapse progress at the same rate. When this process is complete, there is a second step, where the external surfaces undergo kaolinization. Stripping of the tetrahedral sheet only occurs in one of the basal surfaces of each crystal (otherwise one of the external layers in the crystals would consist of an octahedral sheet alone). In this case, the stripping of the tetrahedra and layer collapse progress at the same rate, although, as mentioned above, only 30% of the area is observed by XRD. The reason why in this case there is not an exponential relationship between the two variables is not clear, but it may be related to the geometry of the external kaolinite-like patches, which allow layer collapse in all or most of their surface. These calculations are a good approximation to the experimental results (Fig. 10) and support our interpretation. The model is simple and quantitative, and is based on experimental evidence and plausible assumptions.

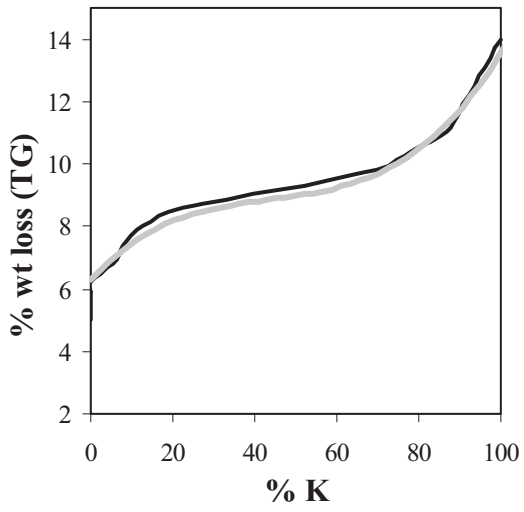

FIGURE 10. Modeling (black line) of the experimental trend in Figure 8 (gray line) representing the relationship between percentage of weight loss due to dehydroxylation of the octahedral sheet and layer collapse to ~7 Å detected by XRD.

The ^{29}Si NMR results show the presence of the kaolinite Si peak (Q^3[0Al]) in samples where no kaolinite was detected by XRD (Fig. 6). This finding is in agreement with the TG results and provides further evidence that there are kaolinite domains in layers that have a smectite d-value. These Q^3(0Al) sites must correspond to Si atoms (with no Al neighbors) in areas where the tetrahedra across the octahedral sheet have been stripped. At this stage, the composition of the octahedral sheet is still smectitic but evidently this has a much smaller effect in the position of the ^{29}Si NMR peak than the stripping of the tetrahedra on the other side of the layer.

Figure 11 shows how the relative area of the kaolinite Si peak evolves with increasing kaolinite content in the four samples analyzed using MAS NMR. Triangles in Figure 11 represent the proportion of kaolinite layers as calculated from XRD results (as in previous plots), and circles represent the percent kaolinite calculated from the % weight loss in the TG experiments. The relative areas of the kaolinite Si NMR peak are in good agreement

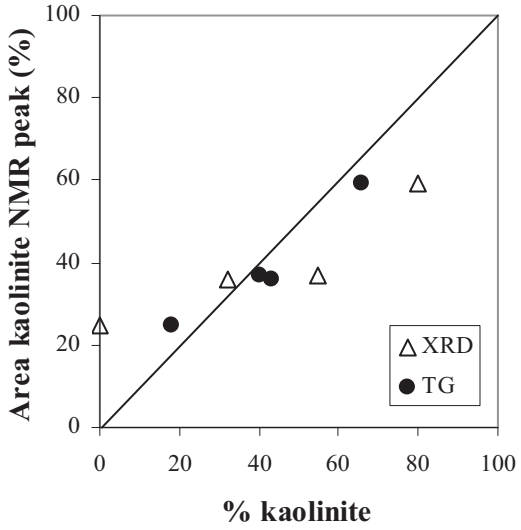

FIGURE 11. Area of the kaolinite ^{29}Si MAS NMR peak at –91 ppm vs. %K measured from XRD (triangles) and TG (circles). There is good agreement between NMR and TG data, but not between the NMR and XRD results. The samples analyzed by NMR (arranged according to increasing %K from XRD) are: TR-4, LT-10/6, LT-2, and RS49.

(diagonal line) with the kaolinite percent as calculated from the TG data (Fig. 11). However, the XRD data are in poor agreement, and the data points take a shape similar to that found in Figure 8 (TG vs. XRD data). This result indicates that the TG and NMR results report the same progress in the smectite kaolinization process. Indeed, this is to be expected because the stripping of tetrahedra and the increase of the number of OH groups are necessarily and immediately linked. For the same reason, when the NMR and XRD data are compared (Fig. 11), the shape of the plot is similar to that of the TG vs. XRD results (Fig. 8).

We considered possible further evidence of the mechanism of kaolinization by relating the number of $Q^2(0Al)$ Si positions with the transformation progress. The growth of kaolinite-like patches should cause an increase of these positions to ~50% kaolinite, and then a decrease as the patches merge and their total perimeter decreases. NMR intensity from the $Q^2(0Al)$ positions contributes to the peak at –87 ppm. The relative intensity of this peak increases from the most smectitic to the most kaolinitic sample (not shown) and, thus, it does not show the expected behavior. The reason for this is that the most kaolinite-rich sample analyzed with NMR (RS49) has a much smaller particle size (<0.2 μm) and thus a much greater contribution to the NMR intensity from the $Q^2(0Al)$ positions at the edges of the crystals than other samples analyzed. An analysis of the evolution of $Q^3(1Al)$ positions is of interest because it would show how the tetrahedral sheet changed composition as the number of Al substituting for Si is reduced. However, such an analysis is not possible because the corresponding signal contributes also to the –87 ppm peak.

In addition to the study by Brindley et al. (1983), already mentioned, Schultz et al. (1971) and Karathanasis and Hajek (1983) also observed a discrepancy between the number of OH groups (dehydroxylation weight loss in TG) and the proportion of kaolinite and smectite in K-S as measured by XRD. Karathanasis and Hajek (1983) studied present-day weathering profiles in Alabama coastal plain sediments showing a transition from smectite to kaolinite and reported an excess of OH groups in beidellites (which, in our view, are smectite-rich kaolinite-smectites, because they formed during transition from montmorillonite to kaolinite and because beidellite is chemically similar to K-S, see Cuadros et al. 1994). According to our interpretation, these samples would correspond to the part of the trend between 0 and ~40 %K in Figure 8. Schultz et al. (1971) noted a deficiency in the structural OH groups in kaolinitic K-S (>50%K) of volcanogenic origin from the Yucatan Peninsula. Their samples represent the section from ~40%K to 100%K in Figure 8. Brindley et al. (1983) suggested that the deficiency of OH groups might be explained by an admixture of very fine-grained smectite that is not detected by XRD, or by defective kaolinite layers "either as regards their lateral extent or their hydroxyl content." Środoń (1999) added the possibility that their XRD mode of layer proportion quantification was incorrect. Our study confirms the correct layer-proportion quantification of previous studies and we provide a reasonable interpretation of these results.

In HRTEM images of K-S samples from the Paris Basin, Amouric and Olives (1998) observed two types of lateral relationships between kaolinite and smectite layers: (1) a transition of one smectite layer into one kaolinite layer, and (2) a transition of one smectite layer into a smectite plus a kaolinite layer. According to Amouric and Olives (1998), the first observation is evidence for a smectite kaolinization mechanism by stripping of one of the tetrahedral sheets. The second observation is interpreted as an intercalation of one kaolinite layer between two smectite layers. Our model of "kaolinite-like patches" finds direct support in the HRTEM images showing a lateral transition from one smectite to one kaolinite layer. However, our results do not provide evidence for or against the second type of relationship between layers observed by Amouric and Olives (1998).

Nature of the "intermediate" component

As shown earlier (Fig. 5), an "intermediate" component was detected and quantified in the DTG curves as the dehydroxylation event that occurs at temperatures intermediate between dehydroxylation of kaolinite and smectite. In Figure 12, the dehydroxylation weight loss of the "intermediate" is plotted vs. the wt% kaolinite in K-S. This wt% kaolinite value was calculated from the % layer composition (%K) assuming the ideal kaolinite composition and an average smectite composition from the apparently pure smectite samples. With increasing amount of kaolinite, the weight loss corresponding to the "intermediate" increases initially, reaches a maximum at about 50 wt% kaolinite, and then decreases.

Combining data from Figures 8 and 12, we interpret the "intermediate" component as the regions of the smectite layers located in direct proximity to the kaolinite-like patches (Fig. 9). Dehydroxylation of the octahedral sheet in these areas occurs at a lower temperature because the diffusion of the evolving H_2O is easier. Thus, the dehydroxylation temperature of these regions is intermediate between those of kaolinite and (unreacted) smectite. The parabolic shape of the trend in Figure 12 occurs because the perimeter of the border between smectite and kaolinite-like patches increases as the area of the patches increases (0–50% kaolinite) and then the perimeter decreases as the kaolinite-like patches merge (50–100% kaolinite). Accord-

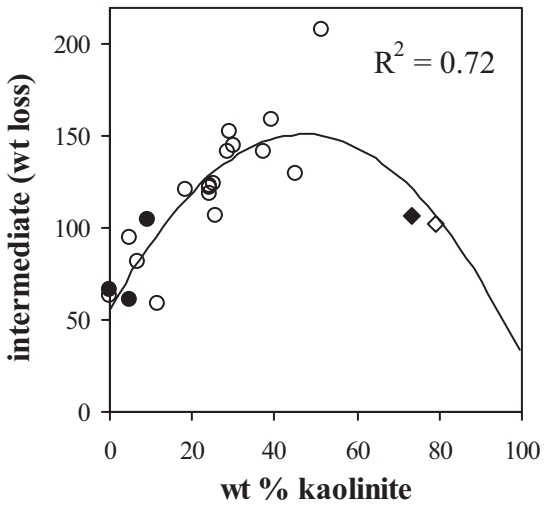

FIGURE 12. Relative amount of weight loss during dehydroxylation at a temperature intermediate between those of kaolinite and smectite, as a function of the percent weight content of kaolinite in K-S (from XRD analysis). Symbols as in Figure 7.

ing to this interpretation, the regression line in Figure 12 should intercept the x axis at 100 wt% kaolinite. This is not the case for two reasons. One is that there are only two samples with wt% kaolinite >50, which places little weight on the descending side of the regression equation. The other reason is that some samples are seemingly composed of two K-S phases of contrasting composition: consider a sample with overall wt% kaolinite <50, but in which one of the K-S phases contains wt% kaolinite >> 50; the latter phase increases the kaolinite content toward 50%, but the corresponding contribution of this phase to the intermediate component is low, because its kaolinite content is high (>>50 wt%) and the perimeter of the kaolinite patches is small. That is, the corresponding data point appears too low in the plot for its wt% kaolinite value. This causes a skewed plot and the regression to flatten, with the result that the high-kaolinite branch of the regression deviates from expected values.

Evolution of the octahedral cation composition

We examined the evolution of the octahedral-cation composition during smectite kaolinization using two complementary approaches. The position of the 06 peak in the XRD patterns (Fig. 13) indicates the *b* dimension of the unit cell, which is related to the octahedral composition owing to differing cation radii (Moore and Reynolds 1997). With increasing %K, the peak migrates from values characteristic of smectite to those of kaolinite. However, the trend is not linear and its shape indicates that the rate of change of the octahedral cation composition during smectite kaolinization (i.e., Al substitution for Mg and Fe) is lower than that of ~7 Å layer formation. Most of the change in the *b* dimension occurs after >60% of the layers have collapsed to ~7 Å.

Based on the chemical analysis, Figure 14 shows changes in Mg and Fe contents with increasing %K. Magnesium is removed gradually as the layers collapse to ~7 Å, however, as the trend is slightly curved, small amounts of Mg might be retained in the kaolinite layers. In contrast, the lack of a trend in the $\%Fe_2O_3$ vs. %K plot implies that Fe remains in the ~7 Å layers or is removed much more slowly than the rate of layer collapse. Hence, Fe is mainly responsible for the non-linear trend in Figure 13. Iron is retained in kaolinite layers and this is another indication that smectite kaolinization proceeds through the inheritance of the original structure. Other studies (Hughes et al. 1993; Carson and Kunze 1967) support this observation, indicating that high Fe content identified in K-S is structurally bound and reflects the high content of this element in the parent smectitic material. Also, Fe-rich kaolinites (to about 1.5 wt% Fe_2O_3; vertical bar in Fig. 14b) have been reported (Weaver 1989; Schroeder and Pruett 1996; Newman and Brown 1987).

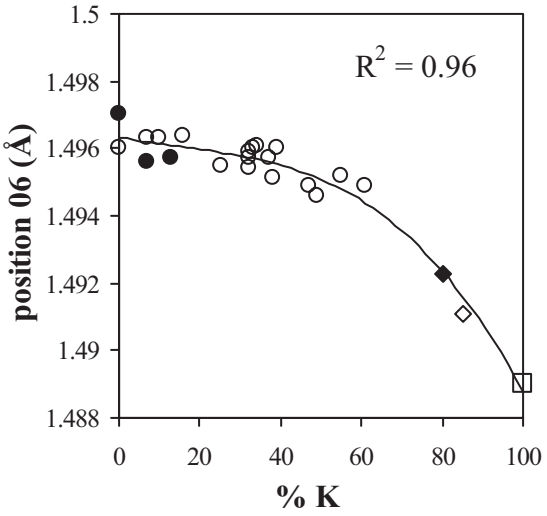

FIGURE 13. Position of the XRD 06 peak as a function of %K in K-S (XRD measurements). Symbols as in Figure 7; square: value for kaolinite from Bailey (1980). The kaolinite value is included in the regression.

Layer-charge evolution

The evolution of the layer charge during the smectite-to-kaolinite reaction may be considered. The layer charge is mirrored by the CEC, i.e., the sum of interlayer cations. Figure 15 shows that %K recorded by XRD and the CEC are not related linearly, with more exchangeable sites in K-S than expected from its smectite content. This trend may indicate that the kaolinite-like patches that are sufficiently large to collapse to ~7 Å retain some layer charge, which could result from residual Mg in the octahedral sheet, as shown in Figure 14a. Also, negative charge in ~7 Å layers may result from residual Al for Si substitution in the tetrahedral sheet. Thus, it appears that kaolinite layers in K-S retain some smectitic character. Hughes et al. (1993) also suggested the possibility that some Al and Fe are accommodated in the tetrahedral sheet of kaolinite layers in K-S.

Alternatively, the non-linear relationship between CEC and %K for our samples can be explained by smectite layers at the crystal edges, which are not detected by XRD but contribute to CEC. Ma and Eggleton (1999) found HRTEM evidence for such smectite layers at the edges of kaolinite crystals in kaolinite with higher than usual CEC values. However, our kaolinite-rich samples have CEC values consistent with their composition.

If there are residual interlayer cations in the ~7 Å layers, they must affect the *d*-value of these layers. The value that produced the best fit in NEWMOD for smectite-rich specimens was 7.4 Å, higher than the usual 7.15 Å for well-crystallized kaolinite. The interlayer cation in our samples is Li with a minimum radius of 0.6 Å (depending on coordination), which is too large for a 7.4 Å spacing if Li is located in the center of the interlayer. However, Li can penetrate the hexagonal cavities of the tetrahedral sheet, thus allowing the layers to come sufficiently close to create 7.4 Å spacings. Also, as the layer charge is small and there is a small number of Li ions in the 7.4 Å interlayers, the surrounding layers could undulate to create a variable *d*-value averaging 7.4 Å. Watanabe et al. (1992) also found the 7.3–7.4 Å *d*-value producing the best fit of the experimental and calculated XRD patterns of their K-S specimens from an acid-clay deposit in Japan. They interpreted the 7.3–7.4 Å component as halloysite on the basis of IR data, because the spectra did not correspond to well-crystallized kaolinite. However, as mentioned above, we expect that the kaolinitic layers in K-S have numerous crystallographic defects and that their IR spectrum is different from that of well-crystallized kaolinite.

CONCLUDING REMARKS

All our evidence indicates that the smectite-to-kaolinite conversion through mixed-layer K-S is a solid-state transformation

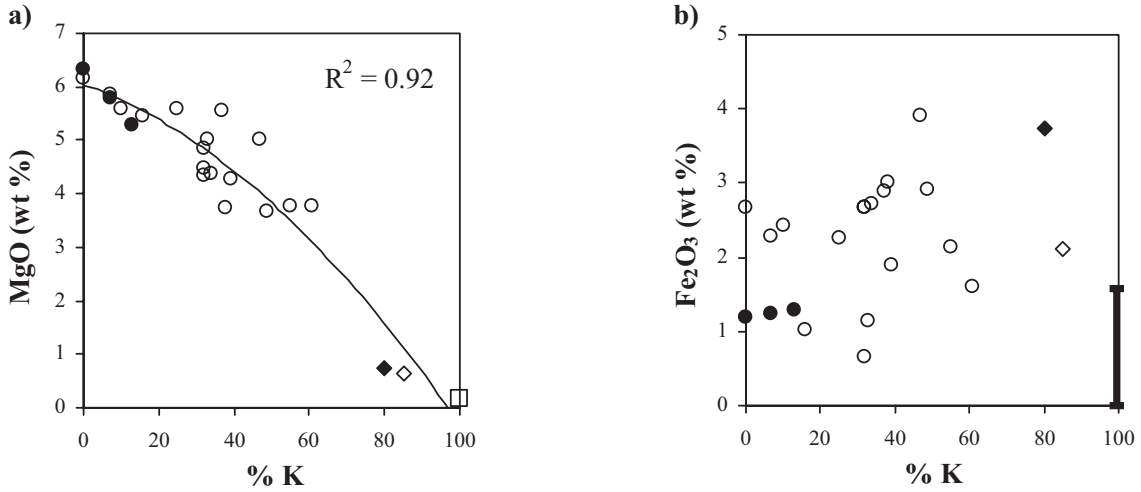

FIGURE 14. (**a**) Mg and (**b**) Fe oxide contents as a function of %K in K-S (from XRD analysis). Symbols as in Figure 13. The kaolinite end-member value in **a** is included in the regression. Vertical bar in **b** is the range of Fe oxide content in kaolinite from the literature (Weaver 1989; Schroeder and Pruett 1996; Newman and Brown 1987).

process requiring several steps. At the initial stage, part of the tetrahedral sheet is removed, releasing Si and some Al, and protons are attached to the O ions in the octahedral sheet, forming OH groups. This leads to the development of kaolinite-like patches, which collapse to ~7 Å only when the size of the patches is sufficiently large. Removal of Mg from the octahedral sheet and its replacement by Al accompanies layer collapse, although it seems that a small amount of Mg remains in the kaolinite layers to preserve some residual layer charge. Some of the Al in the tetrahedral sheet may also be retained and this contributes to the high CEC of the ~7 Å layers. As kaolinization proceeds, the residual octahedral Mg and tetrahedral Al are exchanged by Al and Si, respectively. Finally, Fe seems to be retained in the newly formed kaolinite structure or it is released at a much slower rate than those of the previous steps.

We believe that this process operates in a variety of environments and under a variety of conditions. Our samples were formed by both hydrothermal and hypergenic alteration of bentonite. Other studies of K-S from palaeosols developed on chalk- and silica-rich rocks (Paris Basin, Brindely et al. 1983) (see Fig. 8) and from present-day montmorillonitic soils (Alabama coastal plain, Karathanasis and Hajek 1983) show the same relation between the dehydroxylation weight loss and K-S composition as we present here. Thus, it appears that smectite kaolinization in non-bentonite systems also proceeds through the development of kaolinite-like patches.

No evidence was found for the existence of polar layers in K-S, as this concept is understood in illite-smectite, i.e., 1:1 and 2:1 layers of dual character, smectitic on one side and kaolinitic on the other, so that the tetrahedral and octahedral sheets across every interlayer have both a kaolinitic or both a smectitic composition (for example: ...$OT_S/T_SO_K/T_KOT_S/T_SO$…, where the subscripts indicate a smectitic or a kaolinitic composition). Instead, we found a different type of hybrid between the two types of layers, where structural and chemical changes progress spatially and sequentially. However, polar layers are possible in the same sense established for illite-smectite at some stage during the transformation.

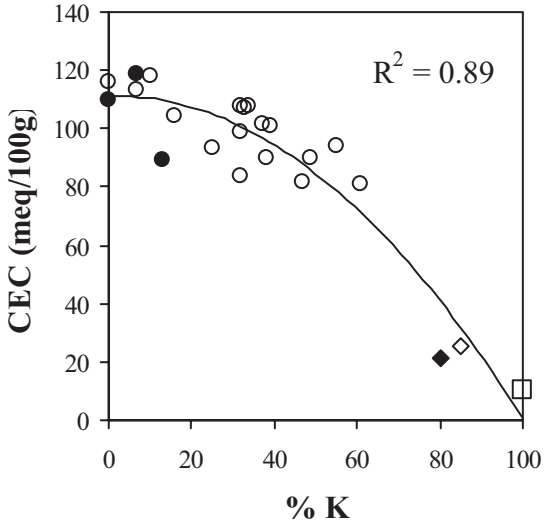

FIGURE 15. Cation exchange capacity (CEC) of K-S as a function of %K in K-S (from XRD analysis). Symbols as in Figure 13. The kaolinite end-member is from Bain and Smith (1994) and is included in the regression.

Note the lack of agreement between the analytical techniques used in this study, when the results are used to quantify the progress of the transformation reaction. We emphasize that each technique provides only partial information. In the case of complex structures involving the interstratification of layers, several techniques are required for characterization. Otherwise, the result may represent a partial picture and cause misinterpretation.

ACKNOWLEDGMENTS

We thank J. Środoń and S. Hillier for supplying two of the samples. We also thank J. Środoń for discussion of the results at an early stage of data interpretation, and S. Hillier, an anonymous reviewer, and S. Guggenheim for their insightful comments and improvements to the final text. Financial support was obtained from The Royal Society-NATO (grant 15144/02B/TB), EPSRC (grant GR/S59772/01) and Marie Curie Fellowship programme (contract MEIF-CT-2003-501678).

REFERENCES CITED

Altaner, S.P., Weiss, C.A., Jr., and Kirkpatrick R.J. (1988) Evidence from ^{29}Si NMR for the structure of mixed-layer illite/smectite clay minerals. Nature, 331, 699–702.

Amouric, M. and Olives J. (1998) Transformation mechanism and interstratification in conversion of smectite to kaolinite: an HRTEM study. Clays and Clay Minerals, 46, 521–527.

Bailey, S.W. (1980) Structures of layer silicates. In G.W. Brindley and G. Brown, Eds., Crystal Structures of Clay Minerals and their X-Ray Identification, p. 2–124. Mineralogical Society, London.

Bain, D.C. and Smith, B.F.L. (1994) Chemical analysis. In M.J. Wilson, Ed., Clay Mineralogy: Spectroscopic and Chemical Determinative Methods, p. 300–332. Chapman & Hall, London.

Brindley, G.W. (1980) Order-disorder in clay mineral structures. In G.W. Brindley and G. Brown, Eds., Crystal Structures of Clay Minerals and their X-Ray Identification, p. 125–196. Mineralogical Society, London.

Brindley, G.W., Suzuki, T., and Thiry, M. (1983) Interstratified kaolinite-smectites from the Paris Basin; correlations of layer proportions, chemical compositions and other data. Bulletin of Mineralogy, 106, 403–410.

Brown, G. and Brindley, G.W. (1980) X-ray diffraction procedures for clay mineral identification. In G.W. Brindley and G. Brown, Eds., Crystal Structures of Clay Minerals and their X-Ray Identification, p. 305–360. Mineralogical Society, London.

Buatier, M.D., Ouyang, K., and Sanchez, J.P. (1993) Iron in hydrothermal clays from the Galapagos Spreading Centre mounds: consequences for the clay transition mechanism. Clay Minerals, 28, 641–655.

Buhmann, C. and Grubb, P.L.C. (1991) A kaolin-smectite interstratification sequence from a red and black complex. Clay Minerals, 26, 343–358.

Carson, C.D. and Kunze, G.W. (1967) Red soils from East Texas developed in glauconitic sediments. Soil Science, 104, 181–190.

Churchman, G.J., Slade, P.G., Self, P.G., and Janik, L.P. (1994) Nature of interstratified kaolin-smectites in some Australian soils. Australian Journal of Soil Research, 32, 805–822.

Cuadros, J. and Altaner, S.P. (1998) Characterization of mixed-layer illite-smectite from bentonites using microscopic, chemical, and X-ray methods: Constraints on the smectite-to-illite transformation mechanism. American Mineralogist, 83, 762–774.

Cuadros, J. and Linares, J. (1995) Some evidence supporting the existence of polar layers in mixed-layer illite/smectite. Clays and Clay Minerals, 43, 467–473.

Cuadros, J., Delgado, A., Cardenete, A., Reyes, E., and Linares, J. (1994) Kaolinite/montmorillonite resembles beidellite. Clays and Clay Minerals, 42, 643–651.

Delvaux, B., Mestdagh, M.M., Vielvoye, L., and Herbillon, A.J. (1989) XRD, IR and ESR study of experimental alteration of Al-nontronite into mixed-layer kaolinite-smectite. Clay Minerals, 24, 617–630.

Hillier, S., Price, R., and Roe, M. (2002) Mixed-layer Kaolinite-smectite from the Jurassic Blisworth Clay, Northamptonshire. 18th General Meeting of International Mineralogical Association, 1–6 September 2002, Edinburgh, Scotland, Abstracts and Program, p. 165.

Hughes, R.E., Moore, D.M., and Reynolds, R.C. (1993) The nature, detection, occurrence, and origin of kaolinite/smectite. In H.H. Murray, W.M. Bundy and C.C. Harvey, Eds., Kaolin genesis and utilisation, p. 291–323. Clay Minerals Society, Boulder, Colorado.

Inoue, A., Velde, B., Meunier, A., and Touchard, G. (1988) Mechanism of illite formation during smectite-to-illite conversion in a hydrothermal system. American Mineralogist, 73, 1325–1334.

Jackson, M.L. (1975) Soil chemical analysis—Advanced course. M. Jackson, Ed., University of Wisconsin, Madison.

Jakobsen, H., Nielsen, N., and Lindgreen, H. (1995) Sequences of charged sheets in rectorite. American Mineralogist, 80, 247–252.

Karathanasis, A.D. and Hajek, B.F. (1983) Transformation of smectite to kaolinite in naturally acid soil systems: Structural and thermodynamic considerations. Soil Science Society of America Journal, 47, 158–163.

Lagaly, G. (1979) The "layer charge" of regular interstratified 2:1 clay minerals. Clays and Clay Minerals, 27, 1–10.

Linares, J. (1985) The process of bentonite formation in Cabo de Gata, Almería, Spain. Mineralogica et Petrographica Acta, 29-A, 17–33.

Lindgreen, H., Jacobsen, H., and Jakobsen, H. (1991) Diagenetic structural transformations in North Sea Jurassic illite-smectite. Clays and Clay Minerals, 39, 54–69.

Ma, C. and Eggleton, R.A. (1999) Surface layer types of kaolinite: A high-resolution transmission electron microscope study. Clays and Clay Minerals, 47, 181–191.

Moore, D.M. and Reynolds, R.C., Jr. (1997) X-ray Diffraction and the Identification and Analysis of Clay Minerals. Oxford University Press, Oxford.

Newman, A.C.D. and Brown, G. (1987) The chemical constitution of clays. In A.C.D. Newman, Ed., Chemistry of Clays and Clay Minerals, p. 1–128. Mineralogical Society, London.

Reyes, E., Huertas, F., and Linares, J. (1978) [Génesis y geoquímica de las esmectitas de Andalucía (España)]. Genesis and geochemistry of the smectites of Andalucia (Spain). Proceedings of the 1st International Congress on Bentonites, Sassari-Calgari, 149–176.

Reynolds, R.C., Jr. and Reynolds, R.C., III (1996) NEWMOD: The Calculation of One-Dimensional X-ray Diffraction Patterns of Mixed-Layer Clay Minerals. Computer Program. 8 Brook Road, Hanover, New Hampshire.

Sakharov, B.A. and Drits, V.A. (1973) Mixed-layer kaolinite-montmorillonite: a comparison of observed and calculated diffraction patterns. Clays and Clay Minerals, 21, 15–17.

Schroeder, P.A. and Pruett, R.J. (1996) Fe ordering in kaolinite: Insights from ^{29}Si and ^{27}Al MAS NMR spectroscopy. American Mineralogist, 81, 26–38.

Schultz, L.G., Shepard, A.O., Blackmon, P.D., and Starkey, H.C. (1971) Mixed-layer kaolinite-montmorillonite from the Yucatan Peninsula, Mexico. Clays and Clay Minerals, 19, 137–150.

Sherriff, B.L., Grundy, H.D., and Hartman, J.S. (1991) The relationship between ^{29}Si MAS NMR chemical shift and silicate mineral structure. European Journal of Mineralogy, 3, 751–768.

Smith, B.F.L. (1994) Characterization of poorly ordered minerals by selective chemical methods. In M.J. Wilson, Ed., Clay Mineralogy: Spectroscopic and Chemical Determinative Methods, p. 333–358. Chapman and Hall, London.

Środoń, J. (1980) Synthesis of mixed-layer kaolinite/smectite. Clays and Clay Minerals, 26, 419–424.

———(1999) Nature of mixed-layer clays and mechanism of their formation and alteration. Annual Review of Earth and Planetary Sciences, 27, 19–53.

Środoń, J., Eberl, D.D., and Drits, V. (2000) Evolution of fundamental particle size during illitization of smectite and implications for the illitization mechanism. Clays and Clay Minerals, 48, 446–459.

Stixrude, L. and Peacor, D. R. (2002) First-principles study of illite-smectite and implications for clay mineral systems. Nature, 420, 165–168.

Theng, B.K.G, Churchman, G.J., and Whitton, J.S. (1984) Comparison of intercalation methods for differentiating halloysite from kaolinite. Clays and Clay Minerals, 32, 249–258.

Trillo, J.M., Alba, M.D., Alvero, R. and Castro, M.A. (1993) Reexpansion of collapsed Li-montmorillonites; Evidence on the location of Li^+ ions. Journal of Chemical Society, Chemical Communications, 24, 1809–1811.

Watanabe, T., Sawada, Y., Russell, J.D., McHardy, W.J., and Wilson, M.J. (1992) The conversion of montmorillonite to interstratified halloysite-smectite by weathering in the Omi acid clay deposit, Japan. Clay Minerals, 27, 159–173.

Weaver, C.E. (1989) Clays, Muds, and Shales. Developments in Sedimentology 44. Elsevier, Amsterdam.

Wiewióra, A. (1973) Mixed-layer kaolinite-smectite from Lower Silesia, Poland: final report. Proceedings of International Clay Conference, Madrid, 1972, 2, 75–88.

MANUSCRIPT RECEIVED JANUARY 13, 2005
MANUSCRIPT ACCEPTED JUNE 6, 2005
MANUSCRIPT HANDLED BY STEPHEN GUGGENHEIM